Theor Chem Acc (2012) 131:1289
DOI 10.1007/s00214-012-1289-5

REGULAR ARTICLE

Time-dependent density functional theory study of charge transfer in collisions

Guillermo Avendaño-Franco · Bernard Piraux · Myrta Grüning · Xavier Gonze

Received: 12 April 2012 / Accepted: 26 September 2012

Abstract We study the charge transfer between colliding ions, atoms, or molecules, within time-dependent density functional theory. Two particular cases are presented, the collision between a proton and a Helium atom, and between a gold atom and a butane molecule. In the first case, proton kinetic energies between 16 keV and 1.2 MeV are considered, with impact parameters between 0.31 and 1.9 Å. The partial transfer of charge is monitored with time. The total cross-section is obtained as a function of the proton kinetic energy. In the second case, we analyze one trajectory and discuss spin-dependent charge transfer between the different fragments.

Keywords Time-dependent density functional theory · Charge transfer · Collisions

Published as part of the special collection of articles celebrating theoretical and computational chemistry in Belgium.

G. Avendaño-Franco · B. Piraux · X. Gonze (✉)
Université Catholique de Louvain (UCL), NAPS-Chemin des étoiles 8 bte L7.03.01, 1348 Louvain-la-Neuve, Belgium
e-mail: xavier.gonze@uclouvain.be

G. Avendaño-Franco
e-mail: guillermo.avendano@uclouvain.be

B. Piraux
e-mail: bernard.piraux@uclouvain.be

M. Grüning
Center for Computational Physics and Physics Department, Universidade de Coimbra, Rua Larga, 3004-516 Coimbra, Portugal
e-mail: myrta@teor.fis.uc.pt

1 Introduction

For more than two decades, density functional theory (DFT) has been used as a reliable tool to describe the electronic structure, total energy, and associated characteristics of molecules and solid-state materials, in the adiabatic approximation [1, 2]. The level of accuracy achieved by DFT is acceptable for a range of purposes in quantum chemistry with a better balance between accuracy and computational cost than more sophisticated approaches based on interacting electronic wave function theory (WFT) [3].

However, quantum chemistry is not restricted to the description of static (or adiabatic) phenomena. Collision dynamics, or the description of systems excited with femtosecond lasers, requires time-dependent approaches. Phenomena like photoionization, excitation, and ionization by electron impact, charge transfer processes [4, 5], atomic scattering, and interstellar chemistry, also call for theoretical support.

For many years, the atomic physics community has been using highly accurate WFT to investigate time-dependent phenomena, including the electronic correlation effects, with impressive success [6]. However, even with present computational resources, only a few electrons can be tackled when such approaches are followed.

Several routes to avoid the treatment of many-body wave functions in collisions, still accounting for adiabatic effects, have been explored. Without being exhaustive, let us mention the approach from Saalmann et al. [7], in which the authors study an exact case with one electron, time-dependent Hartree-Fock (TD-HF), that was used in [8] to explore the charge exchange in the collision $He^{2+} + He$, and many studies based on non-adiabatic hopping between hypersurfaces [9].

Time-dependent density functional theory (TD-DFT) [10] shares with DFT a favorable scaling with the number of electrons and allows one to compute the evolution of the

Published online: 17 October 2012

electronic structure with a time-dependent Hamiltonian, a characteristic that traditionally was only possible from first principles using WFT. In the past few years, TD-DFT has been used by a few groups to study ion–atom collisions : Keim et al. [11] used a basis generator method (BGM) to examine the collisions of bare ions with helium, with excellent agreement with the experimental results from Rudd et al. [12, 13], while Wang et al. [14] examined proton–Argon and proton–Neon [15] collisions, also with reasonable agreement with experimental data. In the latter case, the authors went beyond the analysis of the single electron transfer channel and explored different methods to quantify the double electron transfer. The study of more complex phenomena has been also undertaken recently: collisions between atomic oxygen and graphite clusters [16], and studies of the stopping power of ions impacting on surfaces [17, 18].

Within a long-term effort aiming at the description of the transfer of charges occurring in secondary ion mass spectrometry [19–21], we explore the use of TD-DFT for collisions between ion, atom, and molecule. In the line of Keim, Wang, and coworkers, [11, 14, 15, 22], we examine first the transfer of charge during a simple proton–atom collision, namely the proton–Helium case. We base our analysis on tools that will scale easily to more complex physical situations : the combination of real-space integrated density representation and Hirshfeld partitioning [23] of charge between atoms. Then, we explore the collision between a gold atom and a butane molecule, and apply the same analysis tools. The charge transfer is quantified for each spin channel.

2 Theoretical background

Time-dependent density functional theory (TD-DFT) is an extension of ground-state DFT (GS-DFT) to solve the electronic structure problem under a time-dependent Hamiltonian. Its foundations are similar in purpose to those in GS-DFT, although the set of theorems and their mathematical demonstrations are considerably different. More detailed references about the TD-DFT formalism can be found in [24]. In what follows, we will consider the combination of TD-DFT, for the electronic system, with a classical representation of nuclei motion.

In the presence of a time-dependent Hamiltonian, WFT solves the Schrödinger equation

$$i\frac{\partial}{\partial t}\Psi(\{\mathbf{r}\},t) = \hat{H}(\{\mathbf{r}\},t)\Psi(\{\mathbf{r}\},t), \tag{1}$$

where the Hamiltonian $\hat{H}$ and the wave function Ψ are functions of the spatial coordinates of N electrons $\{\mathbf{r}\} = \{r_1, r_2, \ldots, r_N\}$ and the time. The Hamiltonian is decomposed as:

$$\begin{aligned}\hat{H}(\{\mathbf{r}\},t) &= \hat{T}(\{\mathbf{r}\}) + \hat{W}(\{\mathbf{r}\}) + \hat{V}_{ext}(\{\mathbf{r}\},t)\\ &= -\frac{1}{2}\sum_{i=1}^{N}\nabla_i^2 + \frac{1}{2}\sum_{i,j=1}^{N}\frac{1}{|\mathbf{r}_i - \mathbf{r}_j|}\\ &\quad + \sum_{i=1}^{N} v_{ext}(\mathbf{r}_i,t)\end{aligned} \tag{2}$$

In the case of scattering, without electromagnetic fields, the dependence with time of the Hamiltonian comes from the classical path followed by M point-like nuclei. In such case, the external potential $v_{ext}(\mathbf{r}_i, t)$ can be written:

$$v_{ext}(\mathbf{r},t) = -\sum_{k=1}^{M}\frac{Z_k}{|\mathbf{r} - \mathbf{R}_k(t)|} \tag{3}$$

where Z_k denotes the charge of the nucleus k and $\mathbf{R}_k$ denotes its position.

Once Eq. (1) has been solved, the many-body wave function Ψ defines the electronic density

$$n(\mathbf{r},t) = N\int d^3\mathbf{r}_2 d^3\cdots d^3\mathbf{r}_N |\Psi(\mathbf{r},\mathbf{r}_2,\ldots,\mathbf{r}_N,t)|^2 \tag{4}$$

TD-DFT uses the real scalar field $n(\mathbf{r}, t)$ as the basic variable, instead of the many-body wave function. The foundations of this switch from wave functions to the density as a fundamental quantity comes from the so-called Runge-Gross theorem [10] that establishes a one-to-one correspondence between the external potential $v_{ext}(\mathbf{r}, t)$ and the density $n(\mathbf{r}, t)$. In a similar way as GS-DFT is implemented, TD-DFT also uses an artificial set of non-interacting N wave functions, where the Hamiltonian for each of them is a functional of the time-dependent density. An evolution equation for non-interacting electrons replaces Eq. (1). An initial condition must provided. In our case of collisions between ions, atoms, and/or molecules, we assume that both target and projectile start from their electronic ground state, so that the Hohenberg-Kohn theorem establishes that the ground-state density is sufficient to determine the many-body ground state. Explicitly, let $\phi_i(\mathbf{r}, t)$ be the one-electron orbital, the evolution equation reads :

$$i\frac{\partial}{\partial t}\phi_i(\mathbf{r},t) = \hat{H}_{KS}(\mathbf{r},t)\phi_i(\mathbf{r},t) \tag{5}$$

with the Hamiltonian $\hat{H}_{KS}(\mathbf{r}, t)$ separated in terms of

$$\begin{aligned}\hat{H}_{KS}[n](\mathbf{r},t) &= -\frac{\nabla^2}{2} + v_{ext}(\mathbf{r},t)\\ &\quad + v_{Hartree}[n](\mathbf{r},t) + v_{xc}[n](\mathbf{r},t)\end{aligned} \tag{6}$$

where $v_{Hartree}(\mathbf{r}, t)$ is the classical Hartree potential.

We will rely on the so-called adiabatic local density approximation (ALDA) to describe the exchange-correlation time-dependent functional $v_{xc}[n](\mathbf{r}, t)$, based on the exchange-correlation of a free electron-gas [25–28].

Simulations of collisions were performed using the software package Octopus [29, 30]. Octopus is an implementation of TD-DFT based on a real-space grid discretization. The simulation space is a parallelepiped whose longer axis is along the direction of collision. In general, the projectile and target are placed sufficiently far from each other inside the simulation box. However, for the specific case of proton projectile, the initial position could be also at the frontier or outside the simulation box. The ground state is computed first and used as initial condition for the time evolution. The time evolution is also discretized, the optimal time step is very dependent, not only on the velocity of the ions, but also on the kinetic energy of the electrons. To reduce the number of electrons involved in the dynamics, the description of core electrons is implemented using norm-conserving pseudopotentials (see, e.g., Chap. 11 in [2]). In that case, particular attention has to be paid to avoid overlappings of the cutoff radius of those pseudopotentials that could induce artefacts in the simulation.

During the time evolution, the electrons are treated quantum-mechanically (TD-DFT) and the nuclei are point particles treated classically using a modified Ehrenfest formalism, as described in [31, 32]. The algorithm used to approximate the evolution operator is the approximated enforced time-reversal symmetry (AETRS) as implemented on Octopus. The exponential of the Hamiltonian is expanded using a Krylov subspace approximation of the action of the exponential and the evolution follows the technique described in [33]. The Perdew-Zunger's exchange-correlation [34] is used, and the core electrons are represented using norm-conserving pseudopotentials from Troullier and Martins [36]

3 Proton impacting Helium

Our first case corresponds to the simulation of a collision between a proton and a Helium atom. This is a well-studied problem in atomic physics [11, 13, 37–40], for which a wealth of experimental data as well as results from higher levels of theory are available.

For the simulation, a rectangular parallelepiped of 16.94 Å along the direction of impact and 10.58 Å in the transversal directions is used. The simulation box is defined by its extremes (−8.47, −5.29, −5.29) and (8.47, 5.29, 5.29). The spacing between points in the mesh is 0.1 Bohr (that is, 0.0529 Å). The total number of points in the mesh is $321 \times 201 \times 201 = 12968721$ grid points plus some extra points outside of the boundary to properly compute spatial derivatives.

The Helium atom originally located along the major central axis of the parallelepiped is impacted by a proton that starts in one of the faces of the box with a certain kinetic energy and impact parameter. The starting coordinates for the He target is (−4.2, 0, 0), and for the proton projectile is (−8.47, b, 0), where b is the impact parameter (the perpendicular distance between the path of a projectile and the center of the target)

In scattering processes, usually only the final product of the collision is considered. First principles methods also allow to understand the dynamics during the collision. With the aim to gain understanding of computational as well as physical aspects, we monitor the dynamics of the electronic structure during the entire evolution. However, the amount of data accumulated per time step is quite large, and thus must be handled with care. To fix the idea, the storage of electronic density for 12968721 grid points will require a binary file of about 96 MB. Supposing a total of 25,000 time steps, storing the data each hundred steps will require 24 GB. Instead of storing such amount of data for post-processing purposes only, we decided to introduce small modifications to the Octopus source code to extract the relevant data in a more detailed way during the execution, focusing on selected integrated quantities, described later. Those modifications are only affecting the output of the density : the physics and algorithms implemented in Octopus were not changed.

As the kinetic energy of the proton spans several orders of magnitude, the time step needs to be properly adjusted for each value of kinetic energy. The optimal value was computed for the most energetic proton in such a way that the total energy of the system be constant under a tolerance of 0.03 eV. The larger deviations for the total energy occurs when the proton reaches the closest distance with the He nucleus. After the time step was scaled proportionally for the different energies in such a way that the same number of time steps are needed to move the proton the entire length of the simulation box. The number of time steps required to move the proton from one side of the box to the opposite one is around 30,000. The simulation is stopped at 25,000 time steps when the proton is sufficiently far from the He nucleus and around 3 Å far from the end of the simulation box. At this point, the electronic capture is complete.

As the proton follows its path, coming close to the Helium atom, the electronic structure of the latter is perturbed. Depending on the initial kinetic energy of the projectile and its impact parameter, some charge is ejected out of the Helium atom region and either becomes attached to the proton projectile, or is ejected in all direction of space, including backwards the direction of impact.

In the TD-DFT formalism for a two-electron spin-saturated system such as the Helium atom, only one Kohn-

Sham orbital is explicitly treated. Contrary to WFT, the knowledge of the final state of the system does not allow a unambiguous interpretation of the final result in terms of probabilities of one- and two-electron transfer. However, the one-electron transfer probability is much larger than the two-electron transfer probability, and in the present context, we will assume that the charge density outside the Helium region is a direct image of the one-electron transfer process. This is consistent with the results obtained in [14, 15]

Figure 1 presents several snapshots of the time evolution of the electronic density inside the simulation box, for a typical collision. For the purpose of visualization, the electronic density is integrated in planes perpendicular to the direction of propagation, inside discs of different radii in the $y - z$ plane. One notices that before the collision, the lines for radii larger or equal to $R = 1.59$ Å are undistinguishable from the line obtained in the whole plane, while the spread between different radii increases steadily after the collision, meaning that the electronic charge that is localized within 1.59 Å before the collision, is scattered and occupies the whole simulation box after the collision, as expected.

To measure the amount of charge being transferred to the proton, we integrate the charge around the two nuclei after the scattering and when they are sufficiently separated to measure a stable number of electrons to each of them. In this simulation, the proton carries at the end about 0.4 electrons in a sphere of 1 Å of radius.

In order to examine the stability of the quantitative estimation of the charge transfer, Fig. 2 presents the evolution of the integrated charge in slices of 2 Å, centered on each atom. For completeness, we also present in this graph, the integral of the charge density in the region of space with x lower than -1 (called "Back-scattering slice"), and with x larger than $+1$ (called "Forward-scattering slice").

At the beginning of the simulation, using a slice of 2 Å for the Helium atom, a charge 1.967 electrons is inside the "Helium slice," the charge that spills out of the slice represents the tail of the charge density, split in 0.018

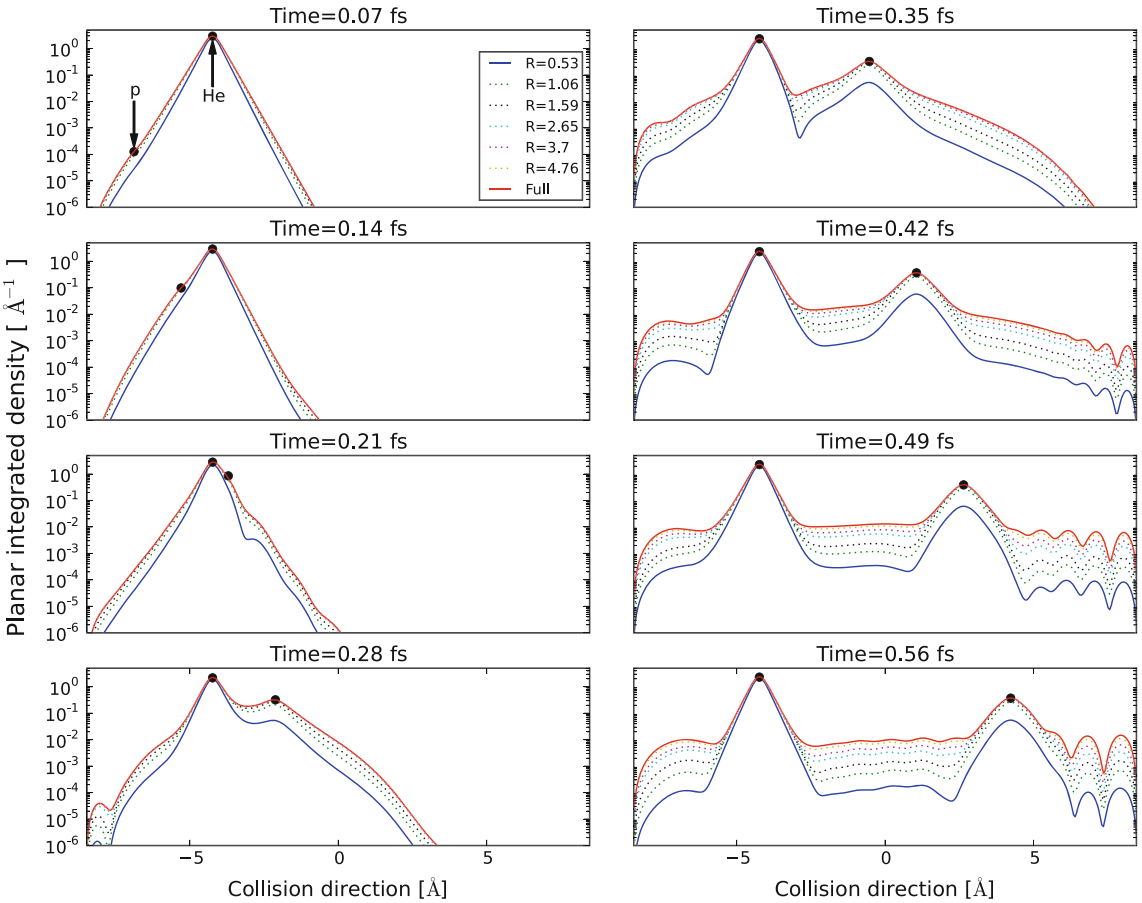

Fig. 1 Snapshots of the integrated planar charge density during a typical proton-Helium collision. The impact parameter is 0.74 Å, the initial kinetic energy of the proton is 26.8 keV. The direction of propagation is x. The *different lines* show the density integrated inside a disc of radius R (in Å) in the $y - z$ plane (or inside the full box) centered on a line that passes through the Helium atom at rest. *Small black dots* are used to show the locations of the nuclei in the direction x (see text)

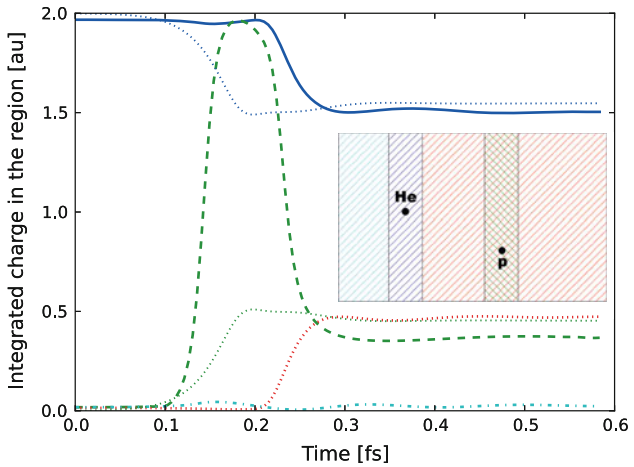

Fig. 2 Amount of charge present in different regions of space during the proton-He collision. The initial kinetic energy and impact parameter are the same than the ones used in Fig. 1. Full line (*blue*) : integrated charge in a slice with x between -5.2 and -3.2, that is, between -1 and $+1$ Å with respect to the Helium atom, defining the "Helium slice". *Dotted line* (*red*): integrated charge with x higher than -3.2, that is, in the "Forward-scattering slice". *Dash-dotted line* (*light blue*): integrated charge with x lower than -3.2, that is, in the "Back-scattering slice". *Dashed line* (*green*): integrated charge in a moving slice, with the difference in x with respect to the proton being between -1 and $+1$, that is, in the "Proton slice". Note that this slice overlaps first with the "Back-scattering slice", then with the "Helium slice", then with the "Forward-scattering slice". *Small dotted line* (*blue*), upper: Hirshfeld charge for the Helium nucleus. *Small dotted line* (*green*), lower: Hirshfeld charge for the proton

electrons for the "Back-scattering slice" and 0.015 electrons for the "Forward-scattering slice." It means that more than 98 % of the charge is initially contained inside the "Helium slice." As the proton gets closer to the Helium, part of the charge associated with the He is also associated with the proton, as the two slices overlap. Finally, when the proton leaves the region of interaction, some charge follows the proton, reducing the charge associated the Helium atom.

The charges associated with proton and He stabilizes around a well-defined value. While the back-scattered charge is quite small, the difference between forward-scattered charge and the charge centered on the proton, after the collision, is non-negligible and calls for further analysis, especially with respect to its angular dependence. Artefacts due to the reflecting nature of the simulation box must also be analyzed. At the end of the time simulation corresponding to Fig. 2, the charge present in the "Back-scattering slice" is 0.023, the charge present in the "Helium slice" is 1.504, the charge present in the "Forward-scattering slice" is 0.473, while the charge present in the "Proton slice" is 0.367.

Figure 2 also presented the Hirshfeld partitioning [23] of the total charge, as a function of time. The Hirshfeld partitioning attributes the charge at each point in space either to the Helium or to the proton, according to a weight that is proportional to the radial densities of the neutral (ground state) Helium or Hydrogen atoms. The implementation of this partitioning is rather easy. Although it completely neglects the possibility that a fraction of electronic charge density might not be attributed to one of both atoms, it constitutes a useful characterization tool that can be transposed easily to more complex situations, as described in the next section [41]. For the present proton–Helium case, after the collision, the Hydrogen Hirshfeld charge is 0.453 and the Helium Hirshfeld charge is 1.547. The Helium Hirshfeld charge is slightly higher than the charge in the "Helium slice." It seems to gather most of the charge excluded from the "Back-scattering slice." Analogously, the proton Hirshfeld charge is larger than the "proton slice charge," and smaller than the charge in the "Forward-scattering slice." In both cases, they stabilize after the collision and can be used to perform an analysis of the transfer of charge.

As seen on Fig. 2, the amount of charge being transferred becomes stable for a given value of initial kinetic energy and impact parameter. The understanding of the long-term evolution of the charge clearly identified to be in the He and H regions seems rather obvious, unlike the charge in other regions.

In Fig. 3, we examine one aspect of the behavior of the charge that remains between the two nuclei. In this respect, we define the planar average velocity as the integral of the local current divided by the local density in the plane perpendicular to the x direction. This figure shows the planar average velocity during the proton–He collision for a reference plane in the scattering region at $x = -0.5$ Å. As the proton approaches the He atom ($t < 0.20$ fs), the charge oscillates at the reference plane, inducing oscillations in the charge velocity. Immediately after the proton–He atom collision ($x = -4.2$ Å, $t = 0.21$ fs), some charge crosses the reference plane, causing a sudden jump in the charge velocity shown in Fig. 3. When the proton crosses the reference plane, ($t = 0.35$ fs), the charge crosses the plane with the same velocity as the proton, as is evident in the plateau found around 0.35 fs. After the crossing of the proton, the velocity of the charge in the plane decreases exponentially. Also, some charge goes back to the Helium atom, visible as a negative value in the current along y. The quantification of the amount of charge going in the different channels (including, e.g., electron scattering) has not been attempted.

Figure 4 gathers the electronic charge transfer values, after collision, as a function of the initial kinetic energy of the projectile, for several values of the impact parameter. Assuming an exponential behavior of the electronic capture as a function of the impact parameter, the capture cross-section based on the proton slice integrated charge density

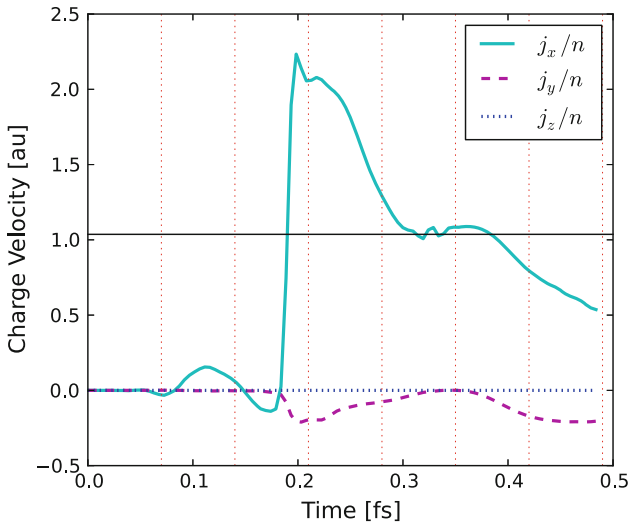

Fig. 3 Components of the planar average charge velocity (*j*/n) as a function of time, for the plane $x = -0.5$ Å. The physical conditions shown here are the same as Fig. 2; the *vertical dashed red lines* indicate the times of the snapshots of Fig. 1. The velocity of the proton is also shown with a *horizontal line*

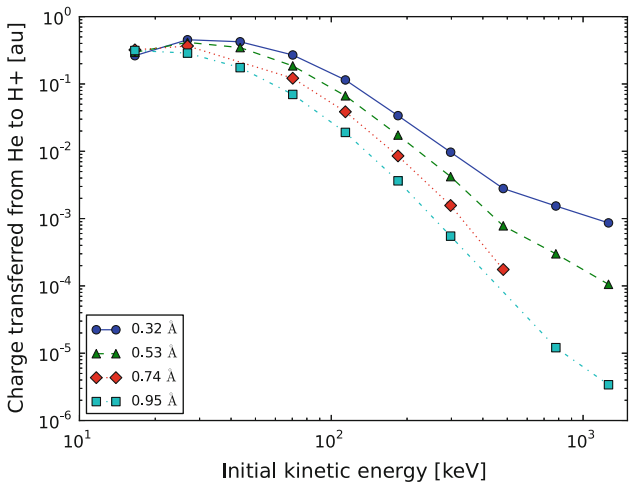

Fig. 4 Electronic charge capture for the proton–Helium collision, as function of the initial kinetic energies for several different impacts parameters. The charge depicted is the charge from the proton slice when the transfer is completed

can be computed as a function of the initial kinetic energy of the projectile. The corresponding data are presented in Fig. 5. There is a good agreement with the experimental data [12, 42–45] in the energy range where they agree (below 150 keV).

One can wonder why the agreement is quite good, although it is well known that TD-DFT usually overestimates charge transfer [46, 47]. However, during collisions, the electronic transfer occurs close to the nuclei, where the electronic density is high. The contribution to the capture cross-section is dominated by collisions with small impact

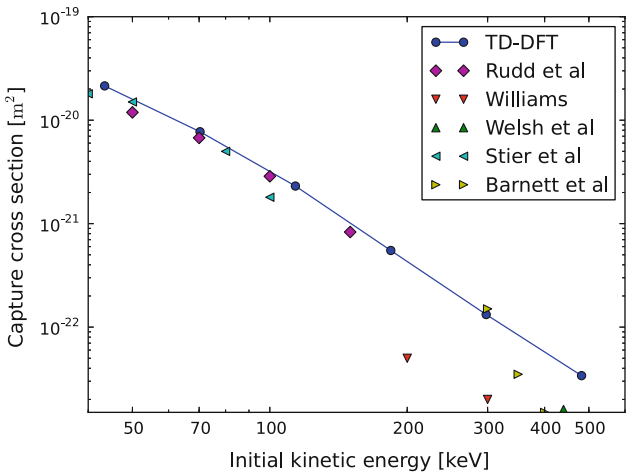

Fig. 5 Electronic capture cross-section by proton in Helium. Experimental results [12, 42–45] are shown for comparison

parameter. The known problem, actually related to the presence of region of spaces weakly populated (exponential decay of the wave function) seems not to be encountered here. Even the lack of a non-local exchange [48] does not affect the capture cross-section. We performed some additional calculations, with the self-interaction correction present in Octopus. We observed that differences in the final outcome of the simulation are negligible.

4 Gold–Butane collision

The collision of an atom of gold and a molecule of butane includes some extra challenges compared with the previous case. Instead of two electrons, now we have a total of 113 electrons. By using pseudopotentials, the number of electrons treated explicitly can be reduced to 37. The gold atom being spin-polarized, we have to treat independently each spin channel. The total number of Kohn-Sham spin orbitals to be handled is thus 37.

As the butane molecule and the gold atom are bigger than the entities of the previous case, the simulation box needs also to be bigger: the box is 22 Å along the direction of collision and 10.5 Å in the transversal directions. As the projectile (Au) now contains electrons, its initial position must be inside of the box.

In the proton–Helium case, the mass ratio between projectile and target was 1:2. With Au as projectile, the proportion is inverted to about 3:1. The simulation presented in Fig. 6 shows an atom of gold, with initial kinetic energy of 23.9 keV, impacting the bond region between two carbon atoms of the butane molecule. We observe that the gold atom breaks the molecule precisely on that bond and continues its path without major deflection. Two fragments are formed from the former butane : one CH_3 ion

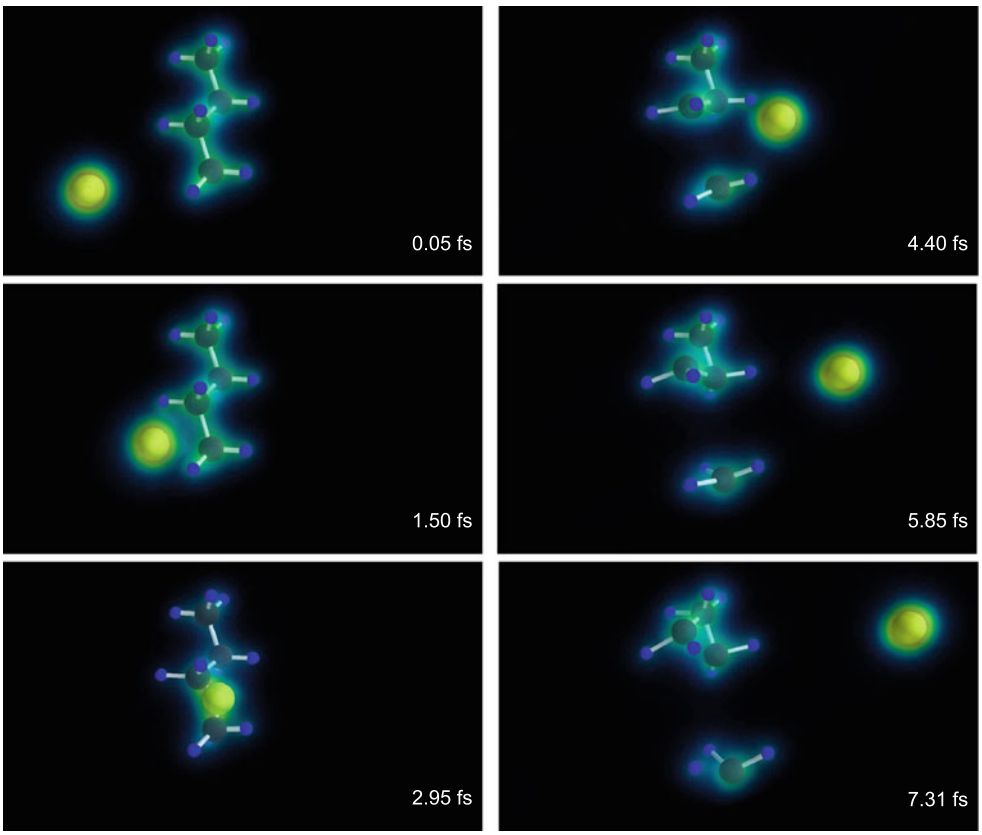

Fig. 6 Snapshots of the collision of a gold atom with a butane molecule. The initial kinetic energy of the projectile is 23.9 keV

(lower part of each sub-figure) and one C_3H_7 ion (upper part of each sub-figure). However, the latter can be seen to decompose in a CH_2 entity (moving upwards), and a C_2H_5 entity (nearly static).

This work is intended to simulate the kind of processes occurring in secondary ion mass spectrometry (SIMS). From a SIMS perspective, the fragmentations present in our simulations should be similar to those occurring in organic polymers due to secondary collision of the atoms from a gold deposit surface as is the case in metal-assisted SIMS (MetA-SIMS). They should have an important role in the ionization of those organic fragments, allowing them to be identified when sputtered.

Following the same methodology than the one used to understand the case of proton and He collision, the planar-integrated density was computed along the direction of impact. It is represented in Fig. 7. As for the proton–Helium collision, such charge density representation allows to visualize the dynamic evolution of the electronic clouds. The two clouds, initially well separated, merge, and then separate, while a small component is present outside of the two major regions.

For kinetic energies as high as in the case presented, and with similarly large impact parameter, the fragments of the butane molecule acquire a relatively small velocity, making easier to partition the charge. We also tested lower kinetic energy cases. However, for some of these, the fragments have a velocity close to the one of the projectile. Measures of charge based on a one-dimensional integrated partition of the space are not as effective. The partition of space must be three-dimensional (as was done with cylinder for the proton–Helium collision) to provide usable results.

In Fig. 8, the Hirshfeld analysis is carried out for each spin component. It shows a well-defined reallocation of the spins charges for the gold atom. As the total amount of charge for each component remains constant, it means that the spin rearrangement is done at expenses of the spin components of the carbon and hydrogen atom. While the charge and spin on the gold atom quickly stabilizes after the collision, on each fragment, the time-dependent Hirshfeld analysis shows some fluctuation between atoms, which is expected (even is confined in a fragment, the electrons continue to oscillate, due to the Ehrenfest dynamics). For a well-separated fragment, like the CH_3 going downwards on Fig. 6, the stabilization is expected to be faster than for each atom separately.

In Table 1, we provide the position, velocity, and Hirshfeld charges (for each spin channel), for each atom, as well as for the C_2H_5, CH_2 and CH_3 fragments, at the

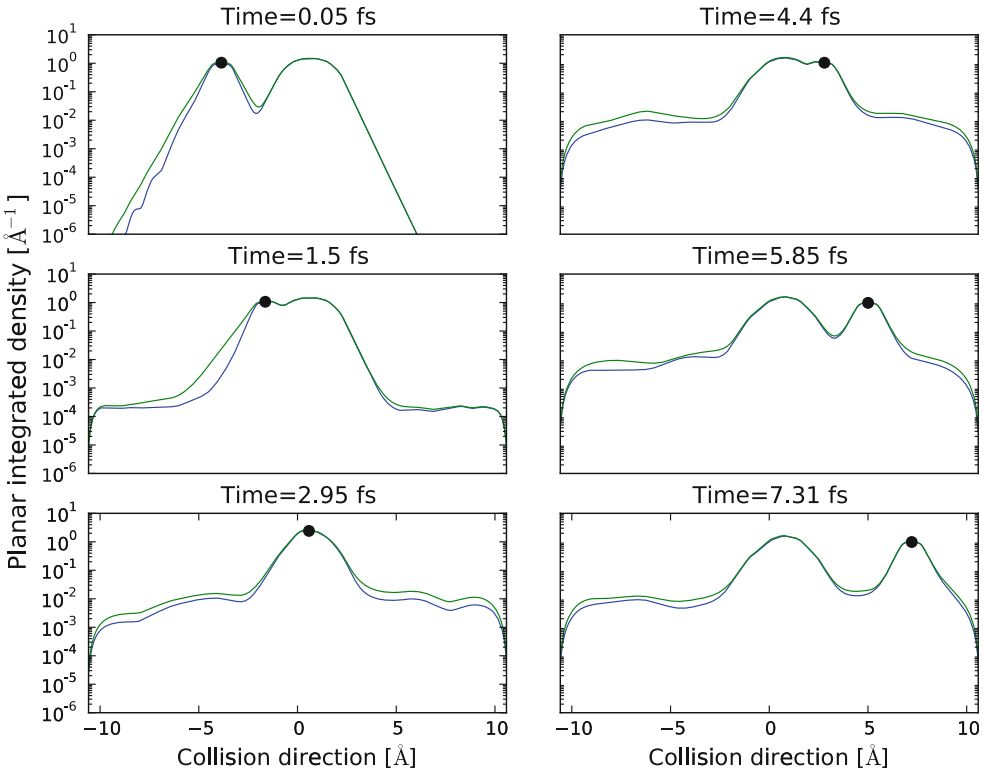

Fig. 7 Planar-integrated charge density, during the simulation of an atom of gold in collision with a butane molecule, corresponding to the six snapshots of Fig. 6. Each spin contribution is considered independently

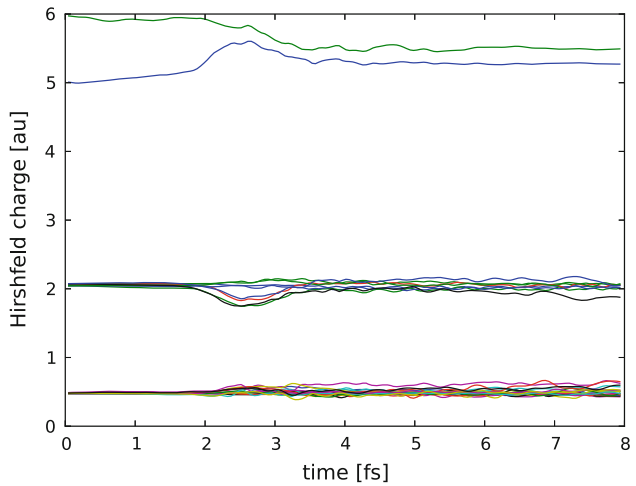

Fig. 8 Evolution of the Hirshfeld charges, during the simulation of the collision between an atom of gold and a butane molecule, with the same parameters as in Fig. 6. Each spin contribution is displayed independently for each atom. The *upper curves* are for the spin up and spin down Hirshfeld charges on the gold atom. The Carbon Hirshfeld charges start at a value of about two (for both spin up and spin down, making four valence electrons for each carbon atom as expected), and the Hydrogen Hirshfeld charges start at a value of about one half (for both spin up and spin down, making one valence electrons for each hydrogen atom as expected)

beginning, and at the end of our simulation. Note that in Fig. 6, the x axis runs diagonal in the perspective of the snapshots. Also, the butane molecule is not symmetric with respect to the impact axis.

The Hirshfeld analysis shows that the gold atom loses a charge of 0.477 electrons in the spin up channel and gains a charge of 0.280 electrons in the spin down channel, with a global loss of 0.197 electrons. The CH_3 fragment charge change (U,D) is (+0.297, −0.135), for a global gain of 0.162 electrons, the CH_2 fragment charge change (U,D) is (+0.134, −0.039), for a global gain of 0.095 electrons, the C_2H_5 fragment charge change (U,D) is (+0.047, −0.106), for a global loss of 0.059 electrons.

5 Conclusions

In the present study, we have analyzed the charge transfer due to collisions, using time-dependent density functional theory. We focused first on the collision of a proton with an atom of Helium, for which we tested analysis tools that would scale also for more complex systems. The agreement with experimental data for scattering cross-section is reasonably good. We apply the same methodology to describe the transfer of charge due to a collision between an atom of gold and a molecule of butane. We find that the slice representation allows for an easy visualization of the whole phenomena, allowing to gauge the charge partitioning in different region of space. The Hirshfeld partitioning yields complementary quantitative information, although the emission of electrons is missing from such representation. In the case of the gold–butane collision, there is a cross-

Table 1 Initial and final conditions for the simulation of a collision between an atom of gold and a molecule of butane

Atom	Initial		Final		
	Position [Å]	Charge (U, D) [a.u.]	Position [Å]	Velocity [Å·fs^{-1}]	Charge (U,D) [a.u]
C	(1.225, 1.773, 0.167)	(2.072, 2.072)	(1.230, 1.789, 0.173)	(2.4e-03, 1.0e-02, 5.7e-03)	(2.065, 2.044)
H	(0.248, 2.202, 0.450)	(0.476, 0.476)	(0.221, 2.229, 0.502)	(−2.7e-03, 2.7e-02, 3.2e-02)	(0.480, 0.464)
H	(1.508, 2.202, −0.811)	(0.476, 0.476)	(1.555, 2.229, −0.855)	(3.5e-02, 2.6e-02, −2.0e-02)	(0.468, 0.444)
H	(1.968, 2.108, 0.909)	(0.475, 0.475)	(2.026, 2.136, 0.972)	(2.3e-02, 1.6e-02, 2.3e-02)	(0.465, 0.460)
C	(1.151, 0.259, 0.093)	(2.045, 2.044)	(1.173, 0.326, 0.170)	(8.8e-03, 1.3e-02, 2.1e-02)	(2.079, 2.041)
H	(0.894, −0.157, 1.086)	(0.477, 0.477)	(0.874, −0.169, 1.174)	(−1.3e-02, −3.1e-03, 1.6e-02)	(0.511, 0.484)
H	(2.145, −0.157, −0.165)	(0.477, 0.476)	(2.466, 0.202, 0.194)	(6.0e-02, 9.7e-02, 9.6e-02)	(0.478, 0.453)
C	(0.136, −0.222, −0.922)	(2.050, 2.042)	(0.393, 1.372, −0.835)	(3.1e-02, 3.3e-01, 1.1e-02)	(2.076, 1.995)
H	(−0.862, 0.180, −0.667)	(0.489, 0.479)	(−0.989, 1.155, −0.394)	(2.4e-02, 1.9e-01, 3.2e-02)	(0.602, 0.558)
H	(0.391, 0.180, −1.921)	(0.477, 0.477)	(0.500, 0.725, −2.230)	(2.2e-02, 1.3e-01, −3.2e-02)	(0.473, 0.407)
C	(0.072, −1.750, −0.987)	(2.075, 2.070)	(0.332, −3.364, −0.967)	(3.9e-02, −3.3e-01, 3.2e-03)	(2.177, 1.844)
H	(−0.206, −2.154, 0.008)	(0.479, 0.477)	(−0.144, −2.656, 0.306)	(3.3e-02, −1.2e-01, 1.7e-02)	(0.545, 0.541)
H	(1.066, −2.154, −1.265)	(0.475, 0.475)	(1.546, −3.125, −1.527)	(7.2e-02, −2.3e-01, −3.6e-02)	(0.508, 0.466)
H	(−0.677, −2.084, −1.735)	(0.481, 0.475)	(−0.700, −2.701, −2.097)	(4.2e-02, −1.3e-01, −8.1e-03)	(0.578, 0.510)
Au	(−3.930, −0.987, −0.987)	(5.972, 5.009)	(7.218, −0.989, −0.998)	(1.5e+00, −8.5e-04, −2.8e-03)	(5.495, 5.289)
C_2H_5	(1.216, 1.055, 0.158)	(6.500, 6.497)	(1.241, 1.104, 0.211)	(8.2e-03, 1.5e-02, 1.6e-02)	(6.547, 6.391)
CH_2	(0.083,−0.165, −0.975)	(3.017, 2.998)	(0.302, 1.310, −0.903)	(3.0e-02, 3.1e-01, 9.2e-03)	(3.151, 2.959)
CH_3	(0.070, −1.826, −0.989)	(3.511, 3.497)	(0.312, −3.257, −0.995)	(4.1e-02,−3.0e-01, 7.4e-04)	(3.808, 3.362)

The gold atom has an initial velocity of 1.53 Å ·fs^{-1} in the positive x direction, and the butane molecule is initially at rest, asymmetrically. The Hirshfeld charge associated to each atom is decomposed into its up (U) and down (D) contribution

exchange of spin charge density between the gold atom and butane molecule (or fragments).

While in the case of the proton–Helium collision, we were able to lead a full sampling of the parameter space (impact parameter, kinetic energy of the projectile), the configuration space for the gold–butane case is much larger, as the orientation of the butane molecule is to be described in a three-parameter space, the whole characterization having to be done in a five-dimensional space. Monte-Carlo techniques should be used to investigate such a parameter space.

Acknowledgments We acknowledge many discussions with A. Delcorte and O. Restrepo related with secondary ion mass spectrometry, and with Y. Popov concerning the proton–Helium collision. This work was supported by the Communauté française de Belgique, through the Action de Recherche Concertée 07/12-003 "Nanosystèmes hybrides metal-organiques", and by the FRS-FNRS Belgium (FRFC Grant 2.4.589.09.F).

References

1. Parr RG, Yang W (1994) Density-functional theory of atoms and molecules. Oxford University Press, New York
2. Martin RM (2004) Electronic structure: basic theory and practical methods. Cambridge University Press, London
3. Matta CF (2010) How dependent are molecular and atomic properties on the electronic structure method? Comparison of Hartree-Fock, DFT, and MP2 on a biologically relevant set of molecules. J Comp Chem 31:1297. doi:10.1002/jcc.21417
4. Yabana K, Tazawa T, Abe Y, Bo zek P (1998) Time-dependent mean-field description for multiple electron transfer in slow ion-cluster collisions. Phys Rev A 57:R3165. doi:10.1103/PhysRevA.57.R3165
5. Kirchner T, Horbatsch M, Lüdde HJ (2002) Time-dependent independent-particle model calculation of multiple capture and ionization processes in $p-\mathrm{Ar}, \overline{p}-\mathrm{Ar}$, and $\mathrm{He}^{2+}-\mathrm{Ar}$ collisions. Phys Rev A 66:052719. doi:10.1103/PhysRevA.66.052719
6. Vanroose W, Martin F, Rescigno TN, McCurdy CW (2005) Complete photo-induced breakup of H_2 molecule as a probe of molecular electron correlation. Science 310:1787. doi:10.1126/science.1120263
7. Saalmann U, Schmidt R (1996) Non-adiabatic quantum molecular dynamics: basic formalism and case study Z. fr. Phys D 38:153. doi:10.1007/s004600050077
8. Kulander KC, Devi KR, Sandhya , Koonin SE (1982) Time-dependent Hartree-Fock theory of charge exchange: Application to He^{2+} + He. Phys Rev A 25:2968. doi:10.1103/PhysRevA.25.2968
9. Tully JC (1990) Molecular dynamics with electronic transitions. J Chem Phys 93:1061. doi:10.1063/1.459170
10. Runge E, Gross EKU (1984) Density-functional theory for time-dependent systems. Phys Rev Lett 52:997. doi:10.1103/PhysRevLett.52.997
11. Keim M, Achenbach A, Lüdde HJ, Kirchner T (2005) Time-dependent density functional theory calculations for collisions of bare ions with helium. Nucl Instrum Meth B 233:240. doi:10.1016/j.nimb.2005.03.114
12. Rudd ME, DuBois RD, Toburen LH, Ratcliffe CA, Goffe TV (1983) Cross sections for ionization of gases by 5-4000-keV protons and for electron capture by 5-150-keV protons. Phys Rev A 28:3244. doi:10.1103/PhysRevA.28.3244

13. Rudd ME, Kim YK, Madison DH, Gallagher JW (1985) Electron production in proton collisions: total cross sections. Rev Mod Phys 57:965. doi:10.1103/RevModPhys.57.965
14. Wang F, Xu XC, Hong XH, Wang J, Gou BC (2011) A theoretical model for electron transfer in ion-atom collisions: calculations for the collision of a proton with an argon atom. Phys Lett A 375:3290. doi:10.1016/j.physleta.2011.07.032
15. Wang F, Hong XH, Wang J, Gou BC, Wang JG (2012) Comparison of three methods for calculation of electron transfer probability in $H^+ + Ne$. Phys Lett A 376:469. doi:10.1016/j.physleta.2011.11.031
16. Isborn CM, Li X, Tully JC (2007) Time-dependent density functional theory Ehrenfest dynamics: collisions between atomic oxygen and graphite clusters. J Chem Phys 126:134307. doi:10.1063/1.2713391
17. Pruneda JM, Sánchez-Portal D, Arnau A, Juaristi JI , Artacho E (2007) Electronic stopping power in LiF from first principles. Phys Rev Lett 99:235501. doi:10.1103/PhysRevLett.99.235501
18. Pruneda JM, Sánchez-Portal D, Arnau A, Juaristi JI, Artacho E (2009) Heating electrons with ion irradiation: a first-principles approach. Nucl Instrum Meth B 267:590. doi:10.1016/j.nimb.2008.11.012
19. Delcorte A, Bour J, Aubriet F, Muller JF, Bertrand P (2003) Sample metallization for performance improvement in desorption/ionization of kilodalton molecules:quantitative evaluation, imaging secondary ion MS, and laser ablation. Anal Chem 75:6875. doi:10.1021/ac0302105
20. Restrepo OA, Prabhakaran A, Hamraoui K, Wehbe N, Yunus S, Bertrand P, Delcorte A (2010) Mechanisms of metal-assisted secondary ion mass spectrometry: a mixed theoretical and experimental study. Surf Interface Anal 42:1030. doi:10.1002/sia.3203
21. Restrepo OA, Delcorte A (2011) Molecular dynamics study of metal-organic samples bombarded by kiloelectronvolt projectiles. Surf Interface Anal 43:70. doi:10.1002/sia.3411
22. Wang F, Hong X, Wang J, Kim KS (2011) Coordinate space translation technique for simulation of electronic process in the ion–atom collision. J Chem Phys 134:154308. doi:10.1063/1.3581820
23. Hirshfeld FL (1977) Bonded-atom fragments for describing molecular charge densities. Theo Chim Acta 44:129. doi:10.1007/BF00549096
24. Marques MAL, Gross EKU (2004) Time-dependent density functional theory. Annu Rev Phys Chem 55:427. doi:10.1146/annurev.physchem.55.091602.094449
25. Marques M, Gross E (2003) In: Fiolhais C, Nogueira F, Marques M (eds) A primer in density functional theory. Springer, Berlin. doi:10.1007/3-540-37072-2
26. Marques M, Ullrich C, Nogueira F, Rubio A, Burke K, Gross EKU (2006) Time-dependent density functional theory. Springer, Berlin. doi:10.1007/b11767107
27. Engel E, Dreizler RM (2011) Density functional theory. Springer, Berlin. doi:10.1007/978-3-642-14090-7
28. Gross EKU, Maitra N (2012) Fundamentals of time-dependent density functional theory. Springer, Berlin. doi:10.1007/978-3-642-23518-4
29. Marques MAL, Castro A, Bertsch GF, Rubio A (2003) Octopus: a first-principles tool for excited electron-ion dynamics. Comput Phys Commun 151:60. doi:10.1016/S0010-4655(02)00686-0
30. Castro A, Heiko A, Oliveira M, Rozzi CA, Andrade X, Lorenzen F, Marques MAL, Gross EKU, Rubio A (2006) Octopus: a tool for the application of time-dependent density functional theory. Phys Status Solidi (b) 243:2465. doi:10.1002/pssb.200642067
31. Alonso JL, Andrade X, Echenique P, Falceto F, Prada-Gracia D, Rubio A (2008) Efficient formalism for large-scale *Ab Initio* molecular dynamics based on time-dependent density functional theory. Phys Rev Lett 101:096403. doi:10.1103/PhysRevLett.101.096403
32. Andrade X, Castro A, Zueco D, Alonso JL, Echenique P, Falceto F, Rubio Ángel (2009) Modified Ehrenfest formalism for efficient large-scale ab initio molecular dynamics. J Chem Theo Comp 5:728. doi:10.1021/ct800518j
33. Castro A, Marques MAL, Rubio A (2004) Propagators for the time-dependent Kohn–Sham equations. J Chem Phys 121:3425. doi:10.1063/1.1774980
34. Perdew JP, Zunger A (1981) Self-interaction correction to density-functional approximations for many-electron systems. Phys Rev B 23:5048. doi:10.1103/PhysRevB.23.5048
35. Perdew JP, Wang Y (1992) Accurate and simple analytic representation of the electron-gas correlation energy. Phys Rev B 45:13244. doi:10.1103/PhysRevB.45.13244
36. Troullier N, Martins JL (1991) Efficient pseudopotentials for plane-wave calculations. Phys Rev B 43:1993. doi:10.1103/PhysRevB.43.1993
37. Belkic D (1978) A quantum theory of ionisation in fast collisions between ions and atomic systems. J Phys B At Mol Phys 11:3529. doi:10.1088/0022-3700/11/20/015
38. Belkic D, Gayet R, Salin A (1979) Electron capture in high-energy ion-atom collisions. Phys Rep 56:279. doi:10.1016/0370-1573(79)90035-8
39. Mergel V, Dörner R, Achler M, Khayyat Kh, Lencinas S, Euler J, Jagutzki O, Nüttgens S, Unverzagt M, Spielberger L, Wu W, Ali R, Ullrich J, Cederquist H, Salin A, Wood CJ, Olson RE, Belkić Dž, Cocke CL, Schmidt-Böcking H (1997) Intra-atomic electron-electron scattering in *p*-He collisions (Thomas Process) investigated by cold target recoil ion momentum spectroscopy. Phys Rev Lett 79:387. doi:10.1103/PhysRevLett.79.387
40. Hasan A, Tooke B, Zapukhlyak M, Kirchner T, Schulz M (2006) Kinematically complete experiment on transfer excitation in intermediate-energy p + He collisions. Phys Rev A 74:032703. doi:10.1103/PhysRevA.74.032703
41. Meister J, Schwarz WHE (1994) Principal components of ionicity. J Phys Chem 98:8245. doi:10.1021/j100084a048
42. Stier PM, Barnett CF (1956) Charge exchange cross sections of hydrogen ions in gases. Phys Rev 103:896. doi:10.1103/PhysRev.103.896
43. Barnett CF, Reynolds HK (1958) Charge exchange cross sections of hydrogen particles in gases at high energies. Phys Rev 109:355. doi:10.1103/PhysRev.109.355
44. Williams JF (1967) Measurement of charge-transfer cross sections for 0.25- to 2.5-MeV protons and hydrogen atoms incident upon hydrogen and helium gases. Phys Rev 157:97. doi:10.1103/PhysRev.157.97
45. Welsh LM, Berkner KH, Kaplan SN, Pyle RV (1967) Cross sections for electron capture by fast protons in H_2, He, N_2, and Ar. Phys Rev 158:85. doi:10.1103/PhysRev.158.85
46. Jamorski C, Foresman JB, Thilgen C, Lüthi HP (2002) Assessment of time-dependent density-functional theory for the calculation of critical features in the absorption spectra of a series of aromatic donor–acceptor systems. J Chem Phys 116:8761. doi:10.1063/1.1465404
47. Dreuw A, Head-Gordon M (2004) Failure of time-dependent density functional theory for long-range charge-transfer excited states: the zincbacteriochlorin bacteriochlorin and bacteriochlorophyll spheroidene complexes. J Am Chem Soc 126:4007. doi:10.1021/ja039556n
48. Dreuw A, Weisman JL, Head-Gordon M (2003) Long-range charge-transfer excited states in time-dependent density functional theory require non-local exchange. J Chem Phys 119:2943. doi:10.1063/1.1590951